TABLE I
COMPARISON OF THEORETICAL RESULTS FOR THE MICROSTRIP ATTENUATION CONSTANT, EXCLUDING GROUND LOSSES, WITH EXPERIMENTAL RESULTS REPORTED BY HYLTIN [16]

Thickness,t (μm)	Atten., α(dB/cm) (Experiment [16])	Atten., α(dB/cm) (Present Method) (No ground losses)
0.254	1.00	0.881
0.508	0.58	0.566
1.524	0.39	0.354
1.778	0.35	0.340
2.286	0.34	0.324
10.160	0.27	0.283

TABLE II
COMPARISON OF THEORETICAL RESULTS FOR THE MICROSTRIP ATTENUATION CONSTANT, INCLUDING GROUND LOSSES, WITH EXPERIMENTAL RESULTS REPORTED BY HYLTIN [16]

Thickness,t (μm)	Atten., α(dB/cm) (Experiment [16])	Atten., α(dB/cm) (Present Method) (With ground losses)
0.254	1.00	0.893
0.508	0.58	0.577
1.524	0.39	0.364
1.778	0.35	0.350
2.286	0.34	0.335
10.160	0.27	0.293

glected. In the second case, Table II the ground losses were included. Our results in these tables are in good agreement with Hyltin's measurements.

IV. CONCLUSION

The effect of the strip conductor thickness on the attenuation constant of microstrip transmission lines has been investigated. Our numerical results are in good agreement with experimental ones obtained from the literature. In agreement with previous studies, it is found that the attenuation is indeed minimized when the thickness to skin depth ratio is about 2, but this is true only for microstrip lines with very large W/H ratios, which are very rarely of any practical interest. We conclude that, for most practical microstrip structures, one cannot rely on a thickness of two skin depths to minimize the attenuation due to conductor losses.

ACKNOWLEDGMENT

The authors would like to thank Dr. J. R. Wait for his valuable comments and fruitful discussions and the reviewers for their constructive critique.

REFERENCES

[1] H. A. Wheeler, "Formulas for the skin depth," *Proc. IRE*, vol. 30, pp. 412–424, Sept. 1942.
[2] Z. Pantic-Tanner and R. Mittra, "Finite-element method for loss calculation in quasi-TEM analysis of microwave transmission lines," *Microwave and Opt. Technol. Lett.*, vol. 1, no. 4, pp. 142–146, June 1988.
[3] D. Mirshekal-Syahkal and J. B. Davies, "Accurate solution of microstrip and coplanar structures for dispersion and for dielectric and conductor losses," *IEEE Trans. Microwave Theory Tech.*, vol. MTT-27, pp. 694–699, July 1979.
[4] J. D. Welch and H. J. Pratt, "Losses in microstrip transmission systems for integrated microwave circuits," *NEREM Rec.*, vol. 8, pp. 100–101. Nov. 1966.
[5] F. Assadourian and E. Rimai, "Simplified theory of microstrip transmission systems," *Proc. IRE*, vol. 40, pp. 1651–1657, Dec. 1952.
[6] R. Horton, B. Easter, and A. Gopinath, "Variation of microstrip losses with thickness of strip," *Electron. Lett.*, vol. 7, no. 17, pp. 490–491, July 1971.
[7] A. C. Cangellaris, "The importance of skin-effect in microstrip lines at high frequencies," in *1988 IEEE MTT-S Int. Microwave Symp. Dig.*, (New York), May 1988, pp. 197–198.
[8] L. P. Vakanas, "An integral equation method for the evaluation of the frequency dependent per unit length inductance and resistance matrices for a uniform multi-conductor lossy transmission line system," MS thesis, Department of Electrical and Computer Engineering, University of Arizona, July 1989.
[9] C. Wei, R. F. Harrington, and T. K. Sarkar, "Multiconductor transmission lines in multilayered dielectric media," *IEEE Trans. Microwave Theory Tech.*, vol. MTT-32, pp. 439–450, Apr. 1984.
[10] G. I. Costache, "Finite element method applied to skin-effect problems in strip transmission lines," *IEEE Trans. Microwave Theory Tech.*, vol. MTT-35, pp. 1009–1013, Nov. 1987.
[11] M. Scheinfein, J. Liao, O. Palusinski, and J. Prince, "Electrical performance of high speed interconnect systems," *IEEE Trans. Components, Hybrids, Manuf. Technol.*, vol. CHMT-10, pp. 303–309, 1987.
[12] J. R. Wait, *Introduction to Antennas and Propagation*. London: P. Peregrinus Ltd., 1986.
[13] M. Caulton and H. Sobol, "Microwave integrated-circuit technology—A survey," *IEEE J. Solid-State Circuits*, vol. SC-5, pp. 292–303, Dec. 1970.
[14] R. A. Pucel, D. J. Masse, and C. P. Hartwig, "Losses in microstrip," *IEEE Trans. Microwave Theory Tech.*, vol. MTT-16, pp. 342–350, June 1968.
[15] R. A. Pucel, D. J. Masse, and C. P. Hartwig, Correction to "Losses in microstrip," *IEEE Trans. Microwave Theory Tech.*, vol. MTT-16, p. 1064, Dec. 1968.
[16] T. M. Hyltin, "Microstrip transmission on semiconductor dielectrics," *IEEE Trans. Microwave Theory Tech.*, vol. MTT-13, pp. 777–781, Nov. 1965.

Frequency-Domain Nonlinear Microwave Circuit Simulation Using the Arithmetic Operator Method

CHAO-REN CHANG AND MICHAEL B. STEER, MEMBER, IEEE

Abstract—**A frequency-domain spectral balance technique for the analysis of microwave circuits with analytically modeled nonlinear devices is developed. The technique uses linear matrix transformation of spectra to perform basic arithmetic operations—multiplication and division—in the frequency domain, and is termed the arithmetic operator method. A single MESFET amplifier described by the Curtice model is simulated with one- and two-tone excitations using this novel technique. Excellent agreement is obtained when compared to the results simulated using the conventional harmonic balance method.**

I. INTRODUCTION

The analysis of nonlinear microwave circuits using frequency-domain spectral balance (FDSB) has been investigated in several different ways, which have included Volterra series expansions [1], [2], algebraic functional expansions [3], [4], and power-series expansions [5], [6]. In general, compared with the conventional harmonic balance (HB) hybrid methods, the FDSB techniques have a larger dynamic range and can be practically used with multitone excitations. However, most FDSB methods are restricted to series representations of nonlinear elements. This has been the major restriction to the widespread use of FDSB techniques. In this paper, we demonstrate a newly developed frequency-domain nonlinear circuit analysis technique, the arith-

Manuscript received October 17, 1989; revised April 3, 1990. This work was supported by a National Science Foundation Presidential Young Investigator Award (Grant ECS-8657836) to M. B. Steer.
The authors are with the Electrical and Computer Engineering Department, North Carolina State University, Raleigh, NC 27695-7911.
IEEE Log Number 9036626.

metic operator method, which is an extension of a generalized power series analysis previously published [7]. Two basic spectral operators—multiplication and division—are introduced. Combined with spectral addition and subtraction, these operators perform their respective arithmetic operations entirely in the frequency domain. Consequently, nonlinear elements described by arbitrary analytic functions in addition to the series representations can be simulated. In Section III, a frequency-domain form of the Curtice MESFET model is presented. Using this model, an FDSB analysis of a MESFET amplifier is compared with a conventional harmonic balance analysis.

II. Arithmetic Operator Method

The arithmetic operator method (AOM) uses basic arithmetic operations on signal spectra in the frequency domain. Here a time-domain signal x is represented in the frequency domain by a spectral vector $\boldsymbol{x}$, defined as

$$\boldsymbol{x} = [X_{0r} X_{1r} X_{1i} \cdots X_{kr} X_{ki} \cdots X_{Kr} X_{Ki}]^T \tag{1}$$

where the frequency-domain components of $\boldsymbol{x}$ are truncated at the radian frequency ω_K and need not be harmonically related. X_{kr} represents the real part of the frequency component of x at ω_k, and X_{ki} is the imaginary part of this component. The phasor of the kth spectrum component is $X_k = X_{kr} + jX_{ki}$. The spectral vectors $\boldsymbol{y}$ and $\boldsymbol{z}$ of the time-domain signals y and z are similarly defined. The basic operations $y = x \pm z$ are implemented in the frequency domain as

$$\boldsymbol{y} = \boldsymbol{x} \pm \boldsymbol{z}. \tag{2}$$

The derivative forms of these operators are equally straightforward. If y, x, and z are all signal u dependent, then the derivative of $\boldsymbol{x}$ with respective to the kth component of $\boldsymbol{u}$ (defined as $\boldsymbol{x}$ in (1)) is

$$\dot{\boldsymbol{x}}_{k,q} = [\partial X_{0r}/\partial U_{k,q} \quad \partial X_{1r}/\partial U_{k,q} \quad \partial X_{1i}/\partial U_{k,q} \cdots \partial X_{Kr}/\partial U_{k,q} \quad \partial X_{Ki}/\partial U_{k,q}]^T \tag{3}$$

where $q = r$ or i indicates the real or the imaginary part. With the spectral vectors $\dot{\boldsymbol{y}}_{k,q}$ and $\dot{\boldsymbol{z}}_{k,q}$ similarly defined, the derivative forms of spectral addition and subtraction are

$$\dot{\boldsymbol{y}}_{k,q} = \dot{\boldsymbol{x}}_{k,q} \pm \dot{\boldsymbol{z}}_{k,q}. \tag{4}$$

Spectral addition and subtraction, and their derivatives, are straightforward as they involve addition or subtraction of the corresponding elements of the spectra operated on. However, more complicated operators, such as multiplication and division, do not only involve corresponding elements, and so the *spectrum mapping function* and the *spectrum transform matrix* must be introduced.

A. Spectrum Mapping Function

In general, a spectrum contains dc, fundamental, harmonic, and intermodulation components, and there is a simple arithmetic relationship of the frequencies of the commensurable spectral components. Here we use a spectrum mapping function to relate the components of the output spectrum to the spectra of two inputs where the output is the product of the two inputs.

Table I is an example of the spectrum mapping function, where $y = xz$ is the system output and x and z are inputs. Three frequency components f_0(= dc), f_1, and f_2(= $2f_1$) are considered here; k_y, k_x, and k_z are frequency indices for the y, x, and z components; and s_x and s_z indicate signs so that

TABLE I
An Example of the Spectrum Mapping Function for the Basic Operation $y = xz$

y	x		z	
k_y	k_x	s_x	k_z	s_z
0	0	+1	0	+1
	1	+1	1	−1
	2	+1	2	−1
1	0	+1	1	+1
	1	+1	0	+1
	1	−1	2	+1
	2	+1	1	−1
2	0	+1	2	+1
	1	+1	1	+1
	2	+1	0	+1

$f_{k_y} = |s_x f_{k_x} + s_z f_{k_z}|$. The k_yth component of the output is then

$$Y_{k_y} = \sum \epsilon X'_{k_x} Z'_{k_z} \tag{5}$$

where

$$\epsilon = \begin{cases} \frac{1}{2} & \text{if } k_x \neq 0 \text{ and } k_z \neq 0 \\ 1 & \text{otherwise} \end{cases} \tag{6}$$

and the k_xth component of x is

$$X'_{k_x} = \begin{cases} X_{k_x} & \text{if } s_{k_x} = +1 \\ X^*_{k_x} & \text{if } s_{k_x} = -1. \end{cases} \tag{7}$$

The term $X^*_{k_x}$ is the complex conjugate of X_{k_x}; Z'_{k_z} is similarly defined; and the summation in (5) is over all rows of the table with the same k_y. The spectrum mapping function is determined using a simple computer program.

Consequently, for a time-domain operation $y = xz$, the spectral vector $\boldsymbol{y}$ can be calculated using (5) and the spectrum mapping function as the linear transformation:

$$\boldsymbol{y} = \boldsymbol{T}_x \boldsymbol{z}.$$

Here the transform matrix $\boldsymbol{T}_x$ is determined using both the spectral vector $\boldsymbol{x}$ and the spectrum mapping function.

B. Spectrum Transform Matrix

The spectrum transform matrix of $\boldsymbol{x}$, $\boldsymbol{T}_x$, is a matrix formulation of the spectrum mapping function for the operation $y = xz$ so that

$$\boldsymbol{y} = \boldsymbol{T}_x \boldsymbol{z}. \tag{8}$$

$\boldsymbol{T}_x$ is formulated using the spectral vector $\boldsymbol{x}$ and its spectrum mapping function only. Element values of $\boldsymbol{T}_x$ are determined by X_k, ϵ, and s, and the location of each element in the matrix is determined by k_y and k_z. $\boldsymbol{T}_x$ is determined using the following algorithm:

$N :=$ the total number of rows of the spectrum mapping function;
$T_x[i,j] := 0$, $(0 \leq i \leq 2K+1,\ 0 \leq j \leq 2K+1)$;
for $n := 0$ **step** 1 **until** $N-1$ **do**
begin
if $k_x \neq 0$ and $k_z \neq 0$ **then** $\epsilon := 0.5$ **else** $\epsilon := 1.0$;
$T_x[2k_y, 2k_z] := T_x[2k_y, 2k_z] + \epsilon X_{k_x,r}$;
$T_x[2k_y, 2k_z+1] := T_x[2k_y, 2k_z+1] - s_x s_z \epsilon X_{k_x,i}$;
$T_x[2k_y+1, 2k_z] := T_x[2k_y+1, 2k_z] + s_x \epsilon X_{k_x,i}$;
$T_x[2k_y+1, 2k_z+1] := T_x[2k_y+1, 2k_z+1] + s_z \epsilon X_{k_x,r}$;
end n loop;

Since the imaginary part of the dc signal is always zero, the second row and the second column of the matrix formulated using the above algorithm are deleted, and the size of T_x is then $(2K+1)\times(2K+1)$. So for the example in Table I,

$$T_x = \frac{1}{2}\begin{bmatrix} 2X_{0r} & X_{1r} & X_{1i} & X_{2r} & X_{2i} \\ 2X_{1r} & 2X_{0r}+X_{2r} & X_{2i} & X_{1r} & X_{1i} \\ 2X_{1i} & X_{2i} & 2X_{0r}-X_{2r} & -X_{1i} & X_{1r} \\ 2X_{2r} & X_{1r} & -X_{1i} & 2X_{0r} & 0 \\ 2X_{2i} & X_{1i} & X_{1r} & 0 & 2X_{0r} \end{bmatrix}. \tag{9}$$

Thus, in the frequency domain, the multiplication operation $y = xz$ is

$$\mathbf{y} = \mathbf{T}_x \mathbf{z} = \mathbf{T}_z \mathbf{x} \tag{10}$$

and its derivative form is

$$\dot{\mathbf{y}}_{k,q} = \mathbf{T}_x \dot{\mathbf{z}}_{k,q} + \mathbf{T}_z \dot{\mathbf{x}}_{k,q}. \tag{11}$$

The spectral division operation is obtained by interchanging y and z. If x is not equal to zero and T_x is a nonsingular matrix, the frequency-domain form of the division operation $y = z/x$ is then

$$\mathbf{y} = \mathbf{T}_x^{-1} \mathbf{z} \tag{12}$$

and its derivative form is

$$\dot{\mathbf{y}}_{k,q} = \mathbf{T}_x^{-1}\left(\dot{\mathbf{z}}_{k,q} - \mathbf{T}_y \dot{\mathbf{x}}_{k,q}\right). \tag{13}$$

Efficient circuit simulation uses Newton's method to iteratively achieve spectral balance. The Jacobian matrix required in this procedure can be calculated using (4), (11), and (13). However, for weak to moderately strong signals, the Jacobian matrix of the spectral vector y with respect to the spectral vector variable x can be evaluated more efficiently and approximated as

$$\mathbf{J}_y(\mathbf{x}) = \mathbf{T}_{y'} \tag{14}$$

where y' is the spectral vector of the derivative of the time-domain analytic function y, dy/dx. This approximated Jacobian matrix is suited to the block Newton convergence scheme [7], where the exact full Jacobian matrix is not always required.

Equations (2), (10), and (12) represent four basic frequency-domain operators: spectral addition, subtraction, multiplication, and division. Theoretically any analytic function can be evaluated in terms of spectral vectors using these basic arithmetic operators. However, they have widely varying calculation efficiencies. Spectral addition and subtraction involve only the straightforward addition or subtraction of the corresponding elements of two vectors. Spectral multiplication requires the formulation of a matrix and then the multiplication of a matrix and a vector. Spectral division, however, is an expensive operation and its use should be minimized as it also requires matrix inversion.

III. The Curtice MESFET Model

The equivalent circuit of the Curtice MESFET model [8], shown in Fig. 1, is commonly used in the harmonic balance analysis of MESFET amplifiers. In this form of the model, C_{gs}, C_{ds}, and C_{gd} are linear and the diodes and transconductance are nonlinear. I_{ds} is modeled as [8]

$$I_{ds} = i_{ds} + i_{rds} \tag{15}$$

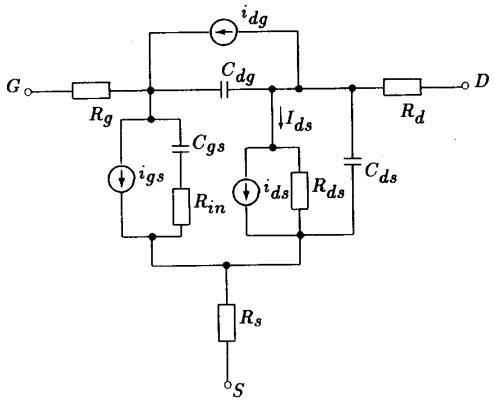

Fig. 1. Equivalent circuit of the Curtice MESFET model.

TABLE II
The Element and Parameter Values of the MESFET Amplifier

Element	Value	Parameter	Value
C_{gs}	0.52785 pF	A_0	0.016542
C_{ds}	0.25137 pF	A_1	0.0500214
C_{dg}	0.087 pF	A_2	0.02012
R_g	2.9 Ω	A_3	−0.00806592
R_{in}	10 Ω	γ	2.16505
R_s	2.4 Ω	A_5	1.0×10^{-12}
R_d	5.3 Ω	β	−0.0394707
		V_{ds}^0	1.0 V
		R_{ds}	218.5 Ω
		I_0	1.0×10^{-9} A
		V_R	15 V

where

$$i_{ds} = \left(A_0 + A_1 v_1 + A_2 v_1^2 + A_3 v_1^3\right)\tanh\left(\gamma v_{ds}\right) \tag{16}$$

$$i_{rds} = \frac{v_{ds} - V_{ds}^{\mathrm{dc}}}{R_{ds}} \tag{17}$$

and

$$v_1 = v_{gs} e^{-j\omega\tau}\left[1 + \beta\left(V_{ds}^0 - v_{ds}\right)\right], \qquad \tau = A_5 v_{ds}. \tag{18}$$

In (15)–(18), the time-domain variables i_{ds}, i_{rds}, v_1, v_{ds}, and v_{gs} are represented by their spectral vector forms, and (15)–(18) are evaluated using the spectral operators.

In [8], the forward-biased gate current i_{gs} and the drain–gate avalanche current i_{dg} are described by piecewise-linear equations. For analytic modeling, we describe these by the Shockley diode equation:

$$i_{gs} = I_0\left(e^{v_{gs}/V_T} - 1\right) \tag{19}$$

and the exponential function:

$$i_{dg} = I_0\left(e^{(v_{dg} - V_R)/V_T} + 1\right) \tag{20}$$

where V_R is the drain–gate reverse breakdown voltage. The values of the linear components and the coefficients in (16)–(20) are listed in Table II.

In the following, the frequency-domain modeling of the Shockley diode equation, the hyperbolic function, and the time delay calculation is presented.

A. Shockley Diode Equation

The exponential function e^x in (19) and (20) is approximated as

$$e^x = \left[1 + \frac{x}{2^n} + \frac{1}{2}\left(\frac{x}{2^n}\right)^2 + \cdots + \frac{1}{n!}\left(\frac{x}{2^n}\right)^n\right]^{2^n}, \qquad n \to \infty \quad (21)$$

where the approximation error for $n \geq 6$ is less than 0.01% over the range $-30 < x < 30$.

The Jacobian matrix of $\boldsymbol{i}_{gs}$ with respect to the variable vector $\boldsymbol{v}_{gs}$ is

$$\boldsymbol{J}_{i_{gs}} = \boldsymbol{T}_{\boldsymbol{y}_{i_{gs}}}, \qquad y_{i_{gs}} = di_{gs}/dv_{gs} \quad (22)$$

where $\boldsymbol{y}_{i_{gs}}$ is the spectral vector of the time-domain variables $y_{i_{gs}}$. The Jacobian matrix of $\boldsymbol{i}_{dg}$ is similarly calculated.

B. Hyperbolic Function

The hyperbolic tangent function $\tanh(\boldsymbol{x})$ can be expressed as

$$\tanh(\boldsymbol{x}) = (1-\boldsymbol{y})/(1+\boldsymbol{y}) \quad (23)$$

where $\boldsymbol{y} = e^{-2\boldsymbol{x}}$ and the Jacobian matrix of the function $\tanh(\boldsymbol{x})$ is

$$\boldsymbol{J}_{\tanh} = \boldsymbol{T}_{\boldsymbol{z}}, \qquad z = 4y/(1+y)^2. \quad (24)$$

C. Time Delay Calculation

In (18), $\boldsymbol{v}_{gs}e^{-j\omega\tau}$ represents the time-delayed gate–source voltage $v_{gs}(t-\tau)$ in the frequency domain, in which τ, in the Curtice model, is a function of the drain–source voltage v_{ds}. This time-delayed signal can be calculated in the frequency domain as follows. If the time-domain signal z represents the time-delayed signal $x(t-y)$, where y is a variable, then z is the real part of the summation of the frequency-domain components of $\boldsymbol{x}$ with their individual phase delays:

$$z = \mathrm{Re}\left\{\sum_{k=0}^{K} X_k e^{j\omega_k t} e^{-j\omega_k y}\right\}. \quad (25)$$

The spectral vector $\boldsymbol{z}$ of z is

$$\boldsymbol{z} = \sum_{k=0}^{K} X_k e^{j\omega_k t} e^{-j\omega_k y}. \quad (26)$$

Since the spectral vector $e^{-j\omega_k y}$ in (26) contains a complex dc component, it cannot be evaluated using (21) and be multiplied by $X_k e^{j\omega_k t}$ using the operator (10). Instead, it is calculated as

$$e^{-j\omega_k y} = \cos(\omega_k y) - j\sin(\omega_k y) \quad (27)$$

and (26) is expressed as

$$\begin{aligned} \boldsymbol{z} &= \sum_{k=0}^{K} \left(X_k e^{j\omega_k t}\{e^{-j\omega_k y}\}_{\mathrm{dc}} + X_k e^{j\omega_k t}\{e^{-j\omega_k y}\}_{\mathrm{ac}}\right) \\ &= \sum_{k=0}^{K} (A_k + B_k) \end{aligned} \quad (28)$$

where $\{e^{-j\omega_k y}\}_{\mathrm{dc}}$ represents the dc component of the spectral vector $e^{-j\omega_k y}$ and is normally a complex number; $\{e^{-j\omega_k y}\}_{\mathrm{ac}}$ represents the ac part and is in a spectral vector form as defined in (1) with a zero dc component. The trigonometric functions in (27) are evaluated using their power-series expansions. With the small value of time delay, a two- or three-term power series is a good approximation. Thus the spectral vector of the time-delayed signal $x(t-y)$ can be performed by calculating A_k and B_k in (28); A_k is a single-tone signal having amplitude $X_k\{e^{-j\omega_k y}\}_{\mathrm{dc}}$ and radian frequency ω_k; B_k is a spectral vector evaluated from the term $X_k e^{j\omega_k t}\{e^{-j\omega_k y}\}_{\mathrm{ac}}$ using the spectral operator (10).

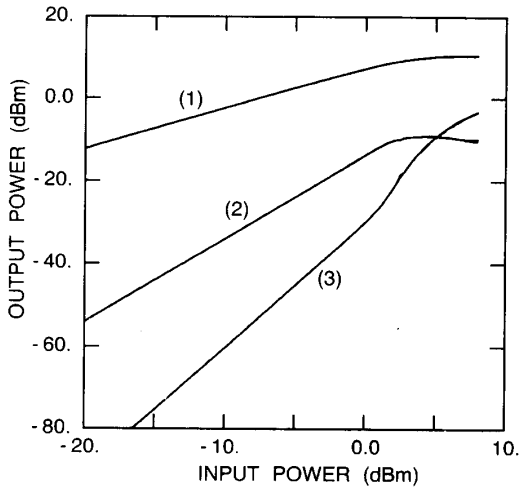

Fig. 2. Comparison of the simulated output power of the single-tone test for the MESFET amplifier using AOM (solid line) and harmonic balance method (dashed line). Shown are the power output at the fundamental (*1*), the second harmonic (*2*), and the third harmonic (*3*) as a function of the input power.

IV. Results and Discussion

Single-tone and two-tone input excitations were used in turn to verify the arithmetic operator method of frequency-domain spectral balance using the MESFET amplifier of [5]. These are compared with the results of an HB simulation using the almost periodic discrete Fourier transform method (APDFT) [9], [10]. With the APDFT-HB method, the time- and frequency-domain nonlinear signals were oversampled to match the accuracy level of that obtained using AOM [11].

Fig. 2 shows the simulated fundamental, second, and third harmonics obtained using AOM (solid line) and APDFT-HB (dashed line) for single-tone excitation. The AOM and APDFT-HB results are almost indistinguishable. With 0 dBm input power and six harmonics considered, the total simulation time for AOM was 0.6 s on a DEC DS3100 RISC workstation (rated at 12-13 VAX 11/780 MIPS).

The two-tone test was set for $f_{\mathrm{LO}} = 2.4$ GHz and $f_{\mathrm{RF}} = 2.35$ GHz. Fig. 3 shows the simulated IF (50 MHz) output power as a function of RF input power. The local oscillator signal was set at -3 dBm, and the RF power varied from -150 dBm to -5 dBm. With a -5 dBm RF signal and second intermodulation order (6 ac, 1 dc) considered, the total simulation time using AOM was 0.7 s. As shown in Fig. 3, the simulated results using the AOM (solid line) and the APDFT-HB method (dashed line) agree for large RF signals. However, at low RF levels, the simulated IF power using the APDFT-HB method deviated from the theoretical straight line and asymptotically approached a constant. The limited dynamic range is inherent in APDFT-HB simulation schemes and is not simply due to frequency truncation [12]. The ultimate dynamic range of an APDFT-HB scheme is determined by numerical accuracy as, in the time domain, a very small signal superimposed on the waveform of a large signal must be representable and then captured by the Fourier transform. In other words, very low level intermodulation distor-

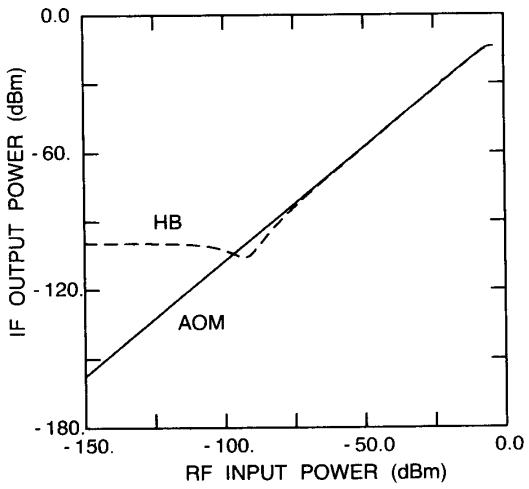

Fig. 3. Comparison of the simulated IF output power of the two-tone test for the MESFET amplifier using AOM (solid line) and harmonic balance method (dashed line). LO power is fixed at −3 dBm.

tion cannot be handled in the presence of a large signal. In contrast, the dynamic range of AOM is determined by the effective accuracy of the Jacobian matrix in the Newton iteration scheme, and here it exceeds 470 dB on the DEC DS3100.

V. Conclusion

In nonlinear analog circuit simulation using the arithmetic operator method, the nonlinear device models are not limited to the series type. This removes the major restriction of frequency-domain spectral balance techniques. Any analytic model can be represented in the frequency domain so that multitone, high-dynamic-range simulation of nonlinear microwave circuits is practical.

References

[1] R. A. Minasian, "Intermodulation distortion analysis of MESFET amplifiers using Volterra series representation," *IEEE Trans. Microwave Theory Tech.*, vol. MTT-28, pp. 1–8, Jan. 1980.

[2] C. L. Law and C. S. Aitchison, "Prediction of wide-band power performance of MESFET distributed amplifiers using the Volterra series representation," *IEEE Trans. Microwave Theory Tech.*, vol. MTT-34, pp. 1308–1317, Dec. 1986.

[3] M. Fliess, M. Lamnabhi, and F. Lamnabhi-Lagarrigue, "An algebraic approach to nonlinear functional expansions," *IEEE Trans. Circuits Syst.*, vol. CAS-30, pp. 554–570, Aug. 1983.

[4] M. Lamnabhi, "Functional analysis of nonlinear circuits: A generating power series approach," *Proc. Inst. Elec. Eng.*, vol. 133, pp. 375–384, Oct. 1986.

[5] G. W. Rhyne, M. B. Steer, and B. D. Bates, "Frequency domain nonlinear circuit analysis using generalized power series," *IEEE Trans. Microwave Theory Tech.*, vol. 36, pp. 379–387, Feb. 1988.

[6] J. H. Haywood and Y. L. Chow, "Intermodulation distortion analysis using a frequency domain harmonic balance technique," *IEEE Trans. Microwave Theory Tech.*, vol. 36, pp. 1251–1257, Aug. 1988.

[7] C. R. Chang, M. B. Steer, and G. W. Rhyne, "Frequency-domain spectral balance using the arithmetic operator method," *IEEE Trans. Microwave Theory Tech.*, vol. 37, pp. 1681–1688, Nov. 1989.

[8] W. R. Curtice and M. Ettenberg, "A nonlinear GaAs FET model for use in the design of output circuits for power amplifiers," *IEEE Trans. Microwave Theory Tech.*, vol. MTT-33, pp. 1383–1393, Dec. 1985.

[9] A. Ushida and L. O. Chua, "Frequency-domain analysis of nonlinear circuits driven by multi-tone signals," *IEEE Trans. Circuits Syst.*, vol. CAS-31, pp. 766–779, Sept. 1984.

[10] K. S. Kundert, G. B. Sorkin, and A. Sangiovanni-Vincentelli, "Applying harmonic balance to almost-periodic circuits," *IEEE Trans. Microwave Theory Tech.*, vol. 36, pp. 366–377, Feb. 1988.

[11] P. L. Heron, C. R. Chang, and M. B. Steer, "Control of aliasing in the harmonic balance simulation of nonlinear microwave circuits," in *1989 IEEE MTT-S Int. Microwave Symp. Dig.*, vol. 1, pp. 355–358.

[12] R. J. Gilmore and M. B. Steer, "Nonlinear circuit analysis using the method of harmonic balance—A review of the art," to appear in *Int. J. Microwave and Millimeter Wave Computer Aided Eng.*, vol. 1, Oct. 1990.